

# Greedy Motion Planning for Simultaneous Signal Landscape Mapping and Receiver Localization

Zaher M. Kassas, *Senior Member, IEEE*, Ari Arapostathis, *Fellow, IEEE*, and Todd E. Humphreys, *Member, IEEE*

**Abstract**—Greedy motion planning strategies to enhance situational awareness in an opportunistic navigation (OpNav) environment is considered. An OpNav environment can be thought of as a radio frequency signal landscape within which a receiver locates itself in time and space by extracting information from ambient signals of opportunity (SOPs). The receiver is assumed to draw only pseudorange observations from the SOPs. The following problem is considered. A receiver with no *a priori* knowledge about its own initial states nor the initial states of multiple SOPs, except for one, is dropped in an OpNav environment. Assuming that the receiver can prescribe its maneuvers, what greedy (i.e., one-step look-ahead) motion planning strategy should the receiver adopt so to optimally build a high-fidelity signal landscape map of the environment while simultaneously localizing itself within this map in time and space with high accuracy? Several information-based and innovation-based motion planning strategies are studied. It is shown that with proper reformulation, the innovation-based strategies can be cast as tractable convex programs, the solution of which is computationally efficient. Simulation results are presented comparing the various strategies and illustrating the improvements gained from adopting the proposed strategies over random and predefined receiver trajectories.

**Index Terms**—Situational awareness, adaptive sensing, trajectory optimization, motion planning, information gathering, navigation, signals of opportunity, opportunistic navigation

## I. INTRODUCTION

Situational awareness is defined as the perception of the elements in the environment within a volume of time and space, the comprehension of their meaning, and the projection of their status in the near future [1]. Reliable and accurate situational awareness is vital in a number of applications, such as autonomous vehicles, disaster management, environmental monitoring, social networks, surveillance, and reconnaissance. Despite the extraordinary advances in global navigation satellite systems (GNSS), their inherent limitations render them unreliable for situational awareness, particularly indoors, in deep urban canyons, and in environments under malicious attacks (e.g., jamming and spoofing) [2], [3].

To overcome the limitations of GNSS and achieve reliable and accurate situational awareness, the outputs of sensors with multiple modalities need to be fused [4], [5]. Motivated by the plenitude of ambient radio frequency signals in GNSS-challenged environments, a new paradigm is emerging [6], [7].

Z.M. Kassas and A. Arapostathis are with the Department of Electrical and Computer Engineering, The University of Texas at Austin. Address: 2501 Speedway, Stop C0803, Austin, TX 78712, USA (email: zkassas@ieee.org and ari@ece.utexas.edu).

T.E. Humphreys is with the Department of Aerospace Engineering and Engineering Mechanics, The University of Texas at Austin. Address: W.R. Woolrich Laboratories, C0600, 210 East 24th Street, Austin, TX 78712, USA (email: todd.humphreys@mail.utexas.edu).

This paradigm, termed opportunistic navigation (OpNav), aims to extract positioning and timing information from ambient radio frequency signals of opportunity (SOPs). These signals include cellular code division multiple access (CDMA) signals [8], digital television vestigial sideband (VSB) signals [9], Iridium satellite time division multiple access (TDMA) signals [10], and orthogonal frequency division multiplexing (OFDM) signals [11]. In collaborative OpNav (COpNav), multiple OpNav receivers share information to construct and continuously refine a global signal landscape [12].

The OpNav estimation problem is similar to the simultaneous localization and mapping (SLAM) problem in robotics [13], [14]. Both imagine an agent which, starting with incomplete knowledge of its location and surroundings, simultaneously builds a map of its environment and locates itself within that map. Typical SLAM environmental maps are stationary. In contrast, the OpNav signal landscape is more complex—it is dynamic and stochastic. The signal landscape map can be thought of metaphorically as a “jello map,” with the jello firmer as the receiver and SOPs clocks are more stable.

The observability of COpNav environments comprising multiple receivers with velocity random walk dynamics making pseudorange measurements on multiple SOPs was thoroughly analyzed in [15], [16], and the degree of observability, also known as estimability, of the various states was quantified in [17]. The effects of allowing receiver-controlled maneuvers on observability was studied in [18]. It was shown that receiver-controlled maneuvers reduce the required *a priori* information about the environment for complete observability, and that the environment is completely observable if the initial state vector of at least one receiver or one “anchor” SOP is fully known. While observability is a Boolean property, i.e. it asserts whether a system is observable or not, it does not specify which trajectory is best for information gathering, and consequently estimability. This is the subject of this paper. To this end, several classical information-based motion strategies are analyzed and novel innovation-based, computationally-efficient strategies are introduced. For the sake of simplicity, this paper considers planar environments. Extensions to three-dimensions is anticipated to be straightforward.

Optimizing an observer’s path in tracking applications has been the subject of extensive research [19]–[21]. In such problems, the observer, which has perfect knowledge about its own states, is tracking a stationary or a mobile target through its onboard sensors. The trajectory optimization objective is to prescribe optimal trajectories for the observer to follow in order to maintain good estimates about the target’s states. In SLAM, the problem of trajectory optimization is more in-

volved, due to the coupling between the localization accuracy and the map quality [22]–[24].

Optimizing the receiver’s trajectory in OpNav environments can be thought of as a hybrid of: (i) optimizing an observer’s path in tracking problems and (ii) optimizing the robot’s path in SLAM [18]. A particular feature of OpNav is that the quality of the estimates not only depends on the spatial trajectory the receiver traverses within the environment, but also on the velocity with which the receiver traverses such trajectory [25].

An initial receiver trajectory optimization study was conducted in [25]. The following problem was considered. A receiver with minimal *a priori* knowledge about its own states and the SOPs’ states is dropped in an OpNav environment. The receiver is assumed to draw pseudorange observations from the SOPs. Assuming that the receiver can prescribe its own maneuvers, what motion planning strategy should the receiver adopt to build a high-fidelity signal landscape map of the environment while simultaneously localizing itself within this map in time and space? To this end, an optimal closed-loop information-theoretic greedy (i.e., one-step look-ahead) receiver motion planning strategy was proposed. Three information measures were studied: D-, A-, and E-optimality. It was demonstrated that all greedy strategies outperformed a receiver moving randomly and in a predefined trajectory. In [18], [26] the greedy motion planning strategy was generalized into a receding horizon (i.e., multi-step look-ahead) trajectory optimization, and the effectiveness and limitations of receding horizon strategy were assessed. Active collaborative signal landscape map building was addressed in [27]. Several information fusion and decision making architectures were studied. It was demonstrated that a hierarchical architecture possessed a negligible “price of anarchy,” which measures the solution quality degradation in a decentralized system from a centralized one.

This paper makes three contributions. The first contribution is to demonstrate that the optimization problems associated with D-, A-, and E-optimality criteria possess no convexity properties, which necessitates relying on general purpose numerical optimization solvers. Subsequently, alternative to these classical information-based measures, innovation-based optimization measures, namely most innovative logarithm-determinant (MILD), most innovative trace (MIT), and most innovative maximum eigenvalue (MIME) are proposed. Innovation-based optimization has not received as much attention in the literature as information-based optimization. The main idea behind innovation-based measures is that one seeks a measurement that is hard to predict, i.e., one with high innovation. To the authors’ knowledge, the only application of innovation-based measures in optimal information gathering appeared in [28], [29]. However, only the eigenvalues of the innovation matrix were considered, which yielded profitable experimental results. Neither analytical nor numerical justifications was provided. The second contribution is to show that with proper reformulations and under mild approximations, MILD, MIT, and MIME possess strong convexity properties, which reduce the optimization problems to searching over the extreme points of the feasibility region. The third contribution is to illustrate the effectiveness

of the proposed strategies through Monte Carlo (MC) simulations and to compare the performance of information-based, innovation-based, random, and predefined motion strategies.

The remainder of this paper is organized as follows. Section II describes the OpNav environment dynamics and observation models. Section III presents optimal information-based and innovation-based greedy motion planning strategies and establishes convexity properties of the innovation-based strategies. Section IV presents simulation results comparing the various strategies. Concluding remarks are given in Section V.

## II. MODEL DESCRIPTION

### A. Dynamics Model

The receiver’s dynamics will be assumed to evolve according to the controlled velocity random walk model. An object moving according to such dynamics in a generic coordinate  $\xi$  has the dynamics

$$\ddot{\xi}(t) = u(t) + \tilde{w}_\xi(t),$$

where  $u(t)$  is the control input in the form of an acceleration command and  $\tilde{w}_\xi(t)$  is a zero-mean white noise process with power spectral density  $\tilde{q}_\xi$ , i.e.,

$$\mathbb{E}[\tilde{w}_\xi(t)] = 0, \quad \mathbb{E}[\tilde{w}_\xi(t)\tilde{w}_\xi(\tau)] = \tilde{q}_\xi \delta(t - \tau),$$

where  $\delta(t)$  is the Dirac delta function. The receiver and SOP clock error dynamics will be modeled according to the two-state model composed of the clock bias  $\delta t$  and clock drift  $\dot{\delta t}$ . The clock error states evolve according to

$$\dot{\mathbf{x}}_{\text{clk}}(t) = \mathbf{A}_{\text{clk}} \mathbf{x}_{\text{clk}}(t) + \tilde{\mathbf{w}}_{\text{clk}}(t),$$

$$\mathbf{x}_{\text{clk}} = \begin{bmatrix} \delta t \\ \dot{\delta t} \end{bmatrix}, \quad \tilde{\mathbf{w}}_{\text{clk}} = \begin{bmatrix} \tilde{w}_{\delta t} \\ \tilde{w}_{\dot{\delta t}} \end{bmatrix}, \quad \mathbf{A}_{\text{clk}} = \begin{bmatrix} 0 & 1 \\ 0 & 0 \end{bmatrix},$$

where the elements of  $\tilde{\mathbf{w}}_{\text{clk}}$  are modeled as zero-mean, mutually independent white noise processes and the power spectral density of  $\tilde{\mathbf{w}}_{\text{clk}}$  is given by  $\mathbf{Q}_{\text{clk}} = \text{diag}[S_{\tilde{w}_{\delta t}}, S_{\tilde{w}_{\dot{\delta t}}}]$ . The power spectra  $S_{\tilde{w}_{\delta t}}$  and  $S_{\tilde{w}_{\dot{\delta t}}}$  can be related to the power-law coefficients  $\{h_\alpha\}_{\alpha=-2}^2$ , which have been shown through laboratory experiments to be adequate to characterize the power spectral density of the fractional frequency deviation  $y(t)$  of an oscillator from nominal frequency, which takes the form  $S_y(f) = \sum_{\alpha=-2}^2 h_\alpha f^\alpha$  [30]. It is common to approximate the clock error dynamics by considering only the frequency random walk coefficient  $h_{-2}$  and the white frequency coefficient  $h_0$ , which lead to  $S_{\tilde{w}_{\delta t}} \approx \frac{h_0}{2}$  and  $S_{\tilde{w}_{\dot{\delta t}}} \approx 2\pi^2 h_{-2}$  [31].

The receiver’s state vector will be defined by augmenting the receiver’s planar position  $\mathbf{r}_r$  and velocity  $\dot{\mathbf{r}}_r$  with its clock error states  $\mathbf{x}_{\text{clk}}$  to yield the state space realization

$$\dot{\mathbf{x}}_r(t) = \mathbf{A}_r \mathbf{x}_r(t) + \mathbf{B}_r \mathbf{u}_r(t) + \mathbf{D}_r \tilde{\mathbf{w}}_r(t), \quad (1)$$

where  $\mathbf{x}_r = [\mathbf{r}_r^\top, \dot{\mathbf{r}}_r^\top, \delta t_r, \dot{\delta t}_r]^\top$ ,  $\mathbf{r}_r = [x_r, y_r]^\top$ ,  $\mathbf{u}_r = [u_1, u_2]^\top$ ,  $\tilde{\mathbf{w}}_r = [\tilde{w}_x, \tilde{w}_y, \tilde{w}_{\delta t_r}, \tilde{w}_{\dot{\delta t}_r}]^\top$ ,

$$\mathbf{A}_r = \begin{bmatrix} \mathbf{0}_{2 \times 2} & \mathbf{I}_{2 \times 2} & \mathbf{0}_{2 \times 2} \\ \mathbf{0}_{2 \times 2} & \mathbf{0}_{2 \times 2} & \mathbf{0}_{2 \times 2} \\ \mathbf{0}_{2 \times 2} & \mathbf{0}_{2 \times 2} & \mathbf{A}_{\text{clk}} \end{bmatrix}, \quad \mathbf{B}_r = \begin{bmatrix} \mathbf{0}_{2 \times 2} \\ \mathbf{I}_{2 \times 2} \\ \mathbf{0}_{2 \times 2} \end{bmatrix}, \quad \mathbf{D}_r = \begin{bmatrix} \mathbf{0}_{2 \times 4} \\ \mathbf{I}_{4 \times 4} \end{bmatrix}.$$

The receiver's dynamics in (1) are discretized at a constant sampling period  $T$  [32]. Assuming zero-order hold of the control inputs, i.e.,  $\{u(t) = u(kT), kT \leq t < (k+1)T\}$ , and dropping  $T$  in the sequel for simplicity of notation yields the discrete-time (DT) model

$$\mathbf{x}_r(k+1) = \mathbf{F}_r \mathbf{x}_r(k) + \mathbf{G}_r \mathbf{u}_r(k) + \mathbf{w}_r(k), \quad k = 0, 1, 2, \dots$$

where  $\mathbf{w}_r$  is a DT zero-mean white noise sequence with covariance  $\mathbf{Q}_r = \text{diag}[\mathbf{Q}_{\text{pv}}, \mathbf{Q}_{\text{clk},r}]$ , where

$$\mathbf{F}_r = \begin{bmatrix} \mathbf{I}_{2 \times 2} & T\mathbf{I}_{2 \times 2} & \mathbf{0}_{2 \times 2} \\ \mathbf{0}_{2 \times 2} & \mathbf{I}_{2 \times 2} & \mathbf{0}_{2 \times 2} \\ \mathbf{0}_{2 \times 2} & \mathbf{0}_{2 \times 2} & \mathbf{F}_{\text{clk}} \end{bmatrix}, \quad \mathbf{G}_r = \begin{bmatrix} \frac{T^2}{2}\mathbf{I}_{2 \times 2} \\ T\mathbf{I}_{2 \times 2} \\ \mathbf{0}_{2 \times 2} \end{bmatrix}, \quad \mathbf{F}_{\text{clk}} = \begin{bmatrix} 1 & T \\ 0 & 1 \end{bmatrix}$$

$$\mathbf{Q}_{\text{clk},r} = \begin{bmatrix} S_{\tilde{w}_{\delta t_r}} T + S_{\tilde{w}_{\delta t_r}} \frac{T^3}{3} & S_{\tilde{w}_{\delta t_r}} \frac{T^2}{2} \\ S_{\tilde{w}_{\delta t_r}} \frac{T^2}{2} & S_{\tilde{w}_{\delta t_r}} T \end{bmatrix}$$

$$\mathbf{Q}_{\text{pv}} = \begin{bmatrix} \tilde{q}_x \frac{T^3}{3} & 0 & \tilde{q}_x \frac{T^2}{2} & 0 \\ 0 & \tilde{q}_y \frac{T^3}{3} & 0 & \tilde{q}_y \frac{T^2}{2} \\ \tilde{q}_x \frac{T^2}{2} & 0 & \tilde{q}_x T & 0 \\ 0 & \tilde{q}_y \frac{T^2}{2} & 0 & \tilde{q}_y T \end{bmatrix}.$$

The SOP will be assumed to emanate from a spatially-stationary terrestrial transmitter whose state consists of its planar position and clock error states. Hence, the SOP's dynamics can be described by the state space model

$$\dot{\mathbf{x}}_s(t) = \mathbf{A}_s \mathbf{x}_s(t) + \mathbf{D}_s \tilde{\mathbf{w}}_s(t), \quad (2)$$

where  $\mathbf{x}_s = [\mathbf{r}_s^\top, \delta t_s, \dot{\delta t}_s]^\top$ ,  $\mathbf{r}_s = [x_s, y_s]^\top$ ,  $\tilde{\mathbf{w}}_s = [\tilde{w}_{\delta t_s}, \tilde{w}_{\dot{\delta t}_s}]^\top$

$$\mathbf{A}_s = \begin{bmatrix} \mathbf{0}_{2 \times 2} & \mathbf{0}_{2 \times 2} \\ \mathbf{0}_{2 \times 2} & \mathbf{A}_{\text{clk}} \end{bmatrix}, \quad \mathbf{D}_s = \begin{bmatrix} \mathbf{0}_{2 \times 2} \\ \mathbf{I}_{2 \times 2} \end{bmatrix}.$$

Discretizing the SOP's dynamics (2) at a sampling interval  $T$  yields the DT-equivalent model

$$\mathbf{x}_s(k+1) = \mathbf{F}_s \mathbf{x}_s(k) + \mathbf{w}_s(k), \quad (3)$$

where  $\mathbf{w}_s$  is a DT zero-mean white noise sequence with covariance  $\mathbf{Q}_s$ , and

$$\mathbf{F}_s = \text{diag}[\mathbf{I}_{2 \times 2}, \mathbf{F}_{\text{clk}}], \quad \mathbf{Q}_s = \text{diag}[\mathbf{0}_{2 \times 2}, \mathbf{Q}_{\text{clk},s}],$$

where  $\mathbf{Q}_{\text{clk},s}$  is identical to  $\mathbf{Q}_{\text{clk},r}$ , except that  $S_{\tilde{w}_{\delta t_r}}$  and  $S_{\tilde{w}_{\dot{\delta t}_r}}$  are now replaced with SOP-specific spectra,  $S_{\tilde{w}_{\delta t_s}}$  and  $S_{\tilde{w}_{\dot{\delta t}_s}}$ , respectively.

### B. Observation Model

To properly model the pseudorange observations, one must consider three different time systems. The first is true time, denoted by the variable  $t$ , which can be considered equivalent to Global Positioning System (GPS) time. The second time system is that of the receiver's clock and is denoted  $t_r$ . The third time system is that of the SOP's clock and is denoted  $t_s$ . The three time systems are related to each other according to

$$t = t_r - \delta t_r(t), \quad t = t_s - \delta t_s(t),$$

where  $\delta t_r(t)$  and  $\delta t_s(t)$  are the amounts by which the receiver and SOP clocks are different from true time, respectively.

The pseudorange observation made by the receiver on an SOP is made in the receiver time and is modeled according to

$$\rho(t_r) = \|\mathbf{r}_r[t_r - \delta t_r(t_r)] - \mathbf{r}_s[t_r - \delta t_r(t_r) - \delta t_{\text{TOF}}]\|_2 + c \cdot \{\delta t_r(t_r) - \delta t_s[t_r - \delta t_r(t_r) - \delta t_{\text{TOF}}]\} + \tilde{v}_\rho(t_r), \quad (4)$$

where  $c$  is the speed of light,  $\delta t_{\text{TOF}}$  is the time-of-flight of the signal from the SOP to the receiver, and  $\tilde{v}_\rho$  is the error in the pseudorange measurement, which is modeled as a zero-mean white Gaussian noise process with power spectral density  $\tilde{r}$  [33]. The clock offsets  $\delta t_r$  and  $\delta t_s$  in (4) were assumed to be small and slowly changing, in which case  $\delta t_r(t) = \delta t_r[t_r - \delta t_r(t)] \approx \delta t_r(t_r)$ . The first term in (4) is the true range between the receiver's position at time of reception and the SOP's position at time of transmission of the signal, while the second term arises due to the offsets from true time in the receiver and SOP clocks.

The observation model in (4) can be further simplified by converting it to true time and invoking mild approximations, discussed in [16], to arrive at

$$\rho(t) \approx \|\mathbf{r}_r(t) - \mathbf{r}_s(t)\|_2 + c \cdot [\delta t_r(t) - \delta t_s(t)] + \tilde{v}_\rho(t), \quad (5)$$

Discretizing the observation equation (5) at a sampling interval  $T$  yields the DT-equivalent observation model

$$\rho(k) = \|\mathbf{r}_r(k) - \mathbf{r}_s(k)\|_2 + c \cdot [\delta t_r(k) - \delta t_s(k)] + v_\rho(k), \quad (6)$$

where  $v_\rho$  is a DT zero-mean white Gaussian sequence with variance  $r = \tilde{r}/T$ .

### C. OpNav Environment Estimator Model

The estimator's dynamics and observation model for an OpNav environment comprising a receiver and multiple SOPs is specified in this subsection. To this end, to satisfy the observability condition established in [18], the knowledge of the initial state vector of one anchor SOP, denoted  $\mathbf{x}_a$ , is assumed. Hence, the estimator's dynamics model is given by

$$\mathbf{x}(k+1) = \mathbf{F} \mathbf{x}(k) + \mathbf{G} \mathbf{u}(k) + \mathbf{w}(k),$$

where  $\mathbf{x} \triangleq [\mathbf{x}_r^\top, \mathbf{x}_{s_1}^\top, \dots, \mathbf{x}_{s_m}^\top]^\top$  is the estimator's state vector,  $\{\mathbf{x}_{s_i}\}_{i=1}^m$  are the state vectors of  $m$  unknown SOPs,  $\mathbf{u} \triangleq \mathbf{u}_r$  is the control vector,  $\mathbf{F} = \text{diag}[\mathbf{F}_r, \mathbf{F}_{s_1}, \dots, \mathbf{F}_{s_m}]$ ,  $\mathbf{G} = [\mathbf{G}_r^\top, \mathbf{0}_{2 \times 4m}]^\top$ , and  $\mathbf{w} \triangleq [\mathbf{w}_r^\top, \mathbf{w}_{s_1}^\top, \dots, \mathbf{w}_{s_m}^\top]^\top$  is a zero-mean process noise vector with covariance  $\mathbf{Q} = \text{diag}[\mathbf{Q}_r, \mathbf{Q}_{s_1}, \dots, \mathbf{Q}_{s_m}]$ . The observation vector has the form  $\mathbf{z} \triangleq [\rho_{s_a}, \rho_{s_1}, \dots, \rho_{s_m}]^\top$ , where  $\rho_{s_j}$  is the pseudorange observation made by the receiver on the  $j$ th SOP, where  $j = a, 1, \dots, m$ . It is assumed that the observation noise elements  $v_{\rho_{s_j}}$  are independent; hence, the estimator's observation noise covariance is given by  $\mathbf{R} = \text{diag}[r_{s_a}, r_{s_1}, \dots, r_{s_m}]$ .

## III. GREEDY MOTION PLANNING

### A. Optimal Receiver Motion Planning Strategy

The objective of the receiver's optimal motion planning is to evaluate different sensing actions that the receiver can take and choose the action that maximizes the information acquired

about the environment while simultaneously minimizing the uncertainty about the receiver's own states. To this end, the one-step look-ahead, also referred to as greedy, receiver motion planning will be considered.

The proposed optimal greedy receiver motion planning loop is depicted in Figure 1, where  $v_{r,\max}$  and  $a_{r,\max}$  are the maximum speed and acceleration, respectively, with which the receiver can move. At a particular time step  $k$ , the pseudorange observations made by the receiver on the various SOPs in the environment,  $z_{s_j}(k)$ ,  $j = a, 1, \dots, m$ , are fused through an estimator, an extended Kalman filter (EKF) in this case, which produces the state estimate  $\hat{\mathbf{x}}(k|k)$  and associated estimation error covariance  $\mathbf{P}(k|k)$ . The estimate and associated covariance are fed to an optimizer. The optimizer solves a nonlinear constrained optimization problem to find the optimal admissible control input  $\mathbf{u}^*(k)$ , which minimizes a functional  $\mathcal{J}$  of the control input, subject to the OpNav environment dynamics and observation models  $\Sigma_{\text{OpNav}}$  and velocity and acceleration constraints. Note that the optimization variable is  $\mathbf{u}(k)$ , whereas  $\mathbf{v}^*(k-1)$  is a known constant vector representing the velocity commands that resulted from solving the optimization problem at the previous time-step  $k-1$  and has already been applied. The optimal control input  $\mathbf{u}^*(k)$  is fed back to the receiver to command its maneuver and is also communicated to the estimator.

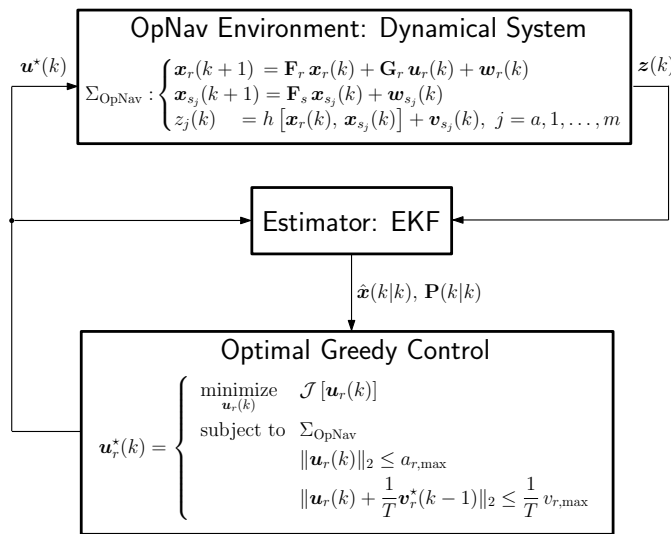


Fig. 1. Optimal greedy receiver motion planning loop

### B. Information and Innovation Optimization Measures

A fundamental challenge in all optimization-based approaches is the choice of a proper optimization metric. This subsection presents various information- and innovation-based optimization metrics. The main issue with these optimization strategies is the dependency of the objective functional on the parameters to be estimated. This issue is prevalent in the literature and is best described by Cochran as: “You tell me the value of  $\theta$ , and I promise to design the best experiment for estimating  $\theta$  [34].”

Information-based metrics are well-established in the literature and are based on the Shannon entropy and Fisher

information. Broadly speaking, Shannon entropy is related to the volume of a set containing a specified probability mass, while Fisher information is related to the surface area of this set [35]. Entropy measures the compactness, and thus the informativeness, of a distribution. The entropy of a random vector  $\mathbf{x}$  with distribution  $p(\mathbf{x})$  is defined as [36]

$$H(\mathbf{x}) \triangleq - \int_{-\infty}^{\infty} p(\mathbf{x}) \log[p(\mathbf{x})] d\mathbf{x}.$$

The mutual information gain after an action  $\mathbf{u}$  is defined as  $\Delta I(\mathbf{u}) \triangleq H(\mathbf{x}) - H(\mathbf{x}|\mathbf{u})$ , where  $H(\mathbf{x}|\mathbf{u})$  is the conditional entropy after action  $\mathbf{u}$ . Thus,  $\Delta I(\mathbf{u})$  is a measure of the reduction in the uncertainty in  $\mathbf{x}$  due to the action  $\mathbf{u}$ . A multivariate Gaussian random vector  $\mathbf{x}$  has entropy proportional to the logarithm of the determinant of its covariance matrix  $\mathbf{P}$ , namely  $H(\mathbf{x}) = \frac{1}{2} \log[(2\pi e)^n \det(\mathbf{P})]$ . Therefore, for a Gaussian random vector  $\mathbf{x}(k)$  with covariance  $\mathbf{P}(k)$ , it can be shown that to maximize the mutual information after an action  $\mathbf{u}(k)$ , one needs to solve the optimization problem

$$\underset{\mathbf{u}(k)}{\text{maximize}} \quad \log \det \left[ \frac{\mathbf{Y}[k+1|\mathbf{u}(k)]}{\mathbf{Y}(k)} \right],$$

where  $\mathbf{Y}(k) \triangleq \mathbf{P}^{-1}(k)$  is the information matrix and  $\mathbf{Y}[k+1|\mathbf{u}(k)]$  is the information matrix after action  $\mathbf{u}(k)$ . Recognizing that  $\mathbf{Y}(k)$  corresponds to the Fisher information matrix, one can establish the connection between Shannon entropy and Fisher information: minimization of Shannon entropy is equivalent to maximization of Fisher information. This is the basis of the so-called D-optimality criterion. Some of the most common information-based optimization measures are defined next [37].

**Definition III.1.** Given an information matrix,  $\mathbf{Y}$ , the D-, A-, and E-optimality criteria are defined as

**D-optimality:** is equivalent to minimization of the volume of the uncertainty ellipsoid, and is given by

$$\text{minimize } \mathcal{J} = -\log \det [\mathbf{Y}].$$

**A-optimality:** is equivalent to minimization of the average variance of the estimates, and is given by

$$\text{minimize } \mathcal{J} = \text{tr} [\mathbf{Y}^{-1}].$$

**E-optimality:** is equivalent to minimization of the length of the largest axis of the uncertainty ellipsoid, and is given by

$$\text{minimize } \mathcal{J} = \lambda_{\max} [\mathbf{Y}^{-1}],$$

where  $\lambda_{\max}$  is the largest eigenvalue.

In contrast to the information-based criteria, which sought to minimize a functional of the information matrix, the innovation-based criteria seek to maximize a functional of the innovation matrix. Intuitively, one seeks the receiver maneuver that yields the most observation innovation, i.e., the “most difficult” observation to predict. This paper introduces the innovation-based optimization criteria: most innovative logarithm-determinant (MILD), most innovative trace (MIT), and most innovative maximum eigenvalue (MIME), which are defined next.

**Definition III.2.** Given an innovation matrix,  $\mathbf{S}$ , the MILD, MIT, and MIME criteria are defined as

**MILD:** is equivalent to maximization of the volume of the innovation ellipsoid, and is given by

$$\text{maximize } \mathcal{J} = \log \det [\mathbf{S}].$$

**MIT:** is equivalent to maximization of the average innovations, and is given by

$$\text{maximize } \mathcal{J} = \text{tr} [\mathbf{S}].$$

**MIME:** is equivalent to maximization of the length of the largest axis of the innovation ellipsoid, and is given by

$$\text{maximize } \mathcal{J} = \lambda_{\max} [\mathbf{S}],$$

where  $\lambda_{\max}$  is the largest eigenvalue.

### C. Information-Based Optimal Motion Planning

The information-based motion planning optimization problems are formulated in this subsection. Given the estimate  $\hat{\mathbf{x}}(k|k)$  and associated estimation error covariance  $\mathbf{P}(k|k)$ , the predicted state vector  $\hat{\mathbf{x}}(k+1|k)$  and associated prediction error covariance  $\mathbf{P}(k+1|k)$  are

$$\begin{aligned} \hat{\mathbf{x}}(k+1|k) &= \mathbf{F}\hat{\mathbf{x}}(k|k) + \mathbf{G}\mathbf{u}(k) \\ \mathbf{P}(k+1|k) &= \mathbf{F}\mathbf{P}(k|k)\mathbf{F}^\top + \mathbf{Q}. \end{aligned}$$

Note that  $\mathbf{P}(k+1|k)$  is not a function of  $\mathbf{u}(k)$ . The observation Jacobian matrix, evaluated at  $\hat{\mathbf{x}}(k+1|k)$ , is given by

$$\mathbf{H} = \begin{bmatrix} \mathbf{h}_1^\top(\hat{\mathbf{r}}_r, \mathbf{u}, \mathbf{r}_{s_a}) & \mathbf{0}_{1 \times 4} & \cdots & \mathbf{0}_{1 \times 4} \\ \mathbf{h}_1^\top(\hat{\mathbf{r}}_r, \mathbf{u}, \hat{\mathbf{r}}_{s_1}) & \mathbf{h}_2^\top(\hat{\mathbf{r}}_r, \mathbf{u}, \hat{\mathbf{r}}_{s_1}) & \cdots & \mathbf{0}_{1 \times 4} \\ \vdots & \vdots & \ddots & \vdots \\ \mathbf{h}_1^\top(\hat{\mathbf{r}}_r, \mathbf{u}, \hat{\mathbf{r}}_{s_m}) & \mathbf{0}_{1 \times 4} & \cdots & \mathbf{h}_2^\top(\hat{\mathbf{r}}_r, \mathbf{u}, \hat{\mathbf{r}}_{s_m}) \end{bmatrix}$$

$$\mathbf{h}_1^\top(\mathbf{r}_r, \mathbf{u}, \mathbf{r}_{s_j}) \triangleq [g_1(\mathbf{r}_r, \mathbf{u}, \mathbf{r}_{s_j}) \quad g_2(\mathbf{r}_r, \mathbf{u}, \mathbf{r}_{s_j}) \quad 0 \quad 0 \quad c \quad 0]$$

$$\mathbf{h}_2^\top(\mathbf{r}_r, \mathbf{u}, \mathbf{r}_{s_j}) \triangleq [-g_1(\mathbf{r}_r, \mathbf{u}, \mathbf{r}_{s_j}) \quad -g_2(\mathbf{r}_r, \mathbf{u}, \mathbf{r}_{s_j}) \quad -c \quad 0]$$

$$g_1(\mathbf{r}_r, \mathbf{u}, \mathbf{r}_{s_j}) \triangleq \frac{x_r + T\dot{x}_r + \frac{T^2}{2}u_1 - x_{s_j}}{\|\mathbf{r}_r + T\dot{\mathbf{r}} + \frac{T^2}{2}\mathbf{u} - \mathbf{r}_{s_j}\|_2}$$

$$g_2(\mathbf{r}_r, \mathbf{u}, \mathbf{r}_{s_j}) \triangleq \frac{y_r + T\dot{y}_r + \frac{T^2}{2}u_2 - y_{s_j}}{\|\mathbf{r}_r + T\dot{\mathbf{r}} + \frac{T^2}{2}\mathbf{u} - \mathbf{r}_{s_j}\|_2},$$

where  $j = a, 1, \dots, m$ , and the time dependency has been dropped above for compactness of notation, namely  $\mathbf{H} = \mathbf{H}(k+1)$ ,  $\hat{\mathbf{r}}_r = \hat{\mathbf{r}}_r(k+1|k)$ ,  $\mathbf{u} = \mathbf{u}(k)$ ,  $\mathbf{r}_{s_a} = \mathbf{r}_{s_a}(k)$ ,  $\hat{\mathbf{r}}_{s_j} = \hat{\mathbf{r}}_{s_j}(k+1|k)$ . The updated covariance matrix is given by

$$\mathbf{P}^{-1}(k+1|k+1) = \mathbf{P}^{-1}(k+1|k) + \mathbf{H}^\top(k+1)\mathbf{R}^{-1}\mathbf{H}(k+1).$$

It is worth noting that  $\mathbf{P}(k+1|k+1)$  is a function of  $\mathbf{u}(k)$  and can be computed without knowledge of the observation at the next time step, namely  $\mathbf{z}(k+1)$ . The cost functional  $\mathcal{J}[\mathbf{u}(k)]$  can be chosen to be the D-, A-, or E-optimality criterion defined in Definition III.1, where  $\mathbf{Y} = \mathbf{P}^{-1}(k+1|k+1)$ .

Ideally, one would like to solve the optimization problem analytically using Lagrange multipliers. However, the problem

quickly becomes intractable as more SOPs are present in the environment. If no analytical solution can be obtained, one typically resorts to numerical optimization solvers. Nevertheless, convexity properties of the problem are sought, if possible, guaranteeing global optimality of the solution and enabling utilization of efficient numerical convex solvers, such as CVX [38]. Plotting  $\mathcal{J}[\mathbf{u}(k)]$  reveals that the D-, A-, and E-optimality criteria are neither convex nor concave as illustrated in Figure 2 for a random OpNav environment comprising a receiver and four SOPs. This necessitates relying on general-purpose numerical constrained nonlinear optimization solvers, which are computationally intensive and may converge to a local minimum.

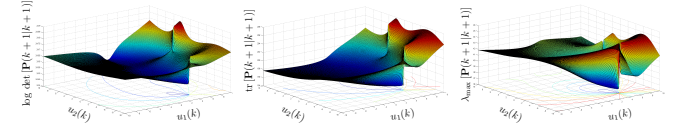


Fig. 2. D-, A-, and E-optimality optimization functionals for an OpNav environment with a receiver and four SOPs.

### D. Innovation-Based Optimal Motion Planning

This subsection formulates the innovation-based optimization problems and shows that with proper reformulation and reasonable approximations such optimization problems have strong convexity properties. Moreover, it is shown that the MILD, MIT, and MIME optimization problems reduce to searching over the extreme points of the feasibility region.

**Theorem III.1.** For a sufficiently small sampling period  $T$  and with proper reformulation, the innovation matrix  $\mathbf{S}(k+1)$  is affine in the control inputs, specifically

$$\mathbf{S}(k+1) = \mathbf{S}_0(k+1) + \sum_{i=1}^2 \mathbf{S}_i(k+1)u_i(k). \quad (7)$$

*Proof:* First, consider transforming the receiver and SOP dynamics in (1)-(2) and observation model in (5) into a polar coordinate frame centered at the receiver  $(x_r, y_r)$ , such that  $(x_j, y_j) \mapsto (r_{s_j}, \theta_{s_j})$ , where  $x_j \triangleq x_r - x_{s_j}$ ,  $y_j \triangleq y_r - y_{s_j}$ , and

$$\begin{cases} r_{s_j} = \sqrt{x_j^2 + y_j^2} \\ \theta_{s_j} = \text{atan2}(y_j, x_j) \end{cases} \Leftrightarrow \begin{cases} x_j = r_{s_j} \cos \theta_{s_j} \\ y_j = r_{s_j} \sin \theta_{s_j} \end{cases}$$

where  $\text{atan2}(y, x)$  is interpreted as the unambiguous four-quadrant arctan function. Hence, the transformed state has the form  $\mathbf{x}' \triangleq \mathbf{g}(\mathbf{x}) = [\xi_{s_a}^\top, \xi_{s_a}^\top, \xi_{s_1}^\top, \xi_{s_1}^\top, \dots, \xi_{s_m}^\top, \xi_{s_m}^\top, \mathbf{x}_{\text{clk}, r}^\top, \mathbf{x}_{\text{clk}, s_1}^\top, \dots, \mathbf{x}_{\text{clk}, s_m}^\top]^\top$ , where  $\xi_{s_j} \triangleq [r_{s_j}, \theta_{s_j}]^\top$ ,  $j = a, 1, \dots, m$ . It can be readily shown that in the transformed coordinate frame the dynamics are nonlinear in the states, yet affine in the control inputs, while the observations are linear time-invariant, specifically

$$\begin{aligned} \dot{\mathbf{x}}'(t) &= \mathbf{f}'_0[\mathbf{x}'(t)] + \sum_{i=1}^2 \mathbf{f}'_i[\mathbf{x}'(t)]u_i(t) + \tilde{\mathbf{w}}'(t) \quad (8) \\ \mathbf{z}(t) &= \mathbf{H}'\mathbf{x}'(t) + \tilde{\mathbf{v}}(t), \end{aligned}$$

$$\begin{aligned} \mathbf{f}'_i &= [\mathbf{f}'_{i,s_a}, \mathbf{f}'_{i,s_1}, \dots, \mathbf{f}'_{i,s_m}, \mathbf{f}'_{i,\text{clk},r}, \mathbf{f}'_{i,\text{clk},s_1}, \dots, \mathbf{f}'_{i,\text{clk},s_m}]^\top \\ \mathbf{f}'_{0,s_j} &= \left[ \dot{r}_{s_j}, \dot{\theta}_{s_j}, r_{s_j} \dot{\theta}_{s_j}^2, \frac{-2\dot{r}_{s_j} \dot{\theta}_{s_j}}{r_{s_j}} \right]^\top, \quad \mathbf{f}'_{0,\text{clk},r} = [\dot{\delta}t_r, 0]^\top \\ \mathbf{f}'_{1,s_j} &= \left[ 0, 0, \cos \theta_{s_j}, \frac{-\sin \theta_{s_j}}{r_{s_j}} \right]^\top, \quad \mathbf{f}'_{0,\text{clk},s_j} = [\dot{\delta}t_{s_j}, 0]^\top \\ \mathbf{f}'_{2,s_j} &= \left[ 0, 0, \sin \theta_{s_j}, \frac{\cos \theta_{s_j}}{r_{s_j}} \right]^\top \\ \mathbf{f}'_{1,\text{clk},r} &= \mathbf{f}'_{1,\text{clk},s_j} = \mathbf{f}'_{2,\text{clk},r} = \mathbf{f}'_{2,\text{clk},s_j} = \mathbf{0}_{2 \times 1} \\ \tilde{\mathbf{w}}' &= [\tilde{\mathbf{w}}'_{s_a}, \tilde{\mathbf{w}}'_{s_1}, \dots, \tilde{\mathbf{w}}'_{s_m}, \tilde{\mathbf{w}}'_{\text{clk},r}, \tilde{\mathbf{w}}'_{\text{clk},s_1}, \dots, \tilde{\mathbf{w}}'_{\text{clk},s_m}]^\top \\ \tilde{\mathbf{w}}'_{s_j} &= [0, 0, \tilde{w}'_{1,s_j}, \tilde{w}'_{2,s_j}]^\top, \end{aligned}$$

where  $i = 0, 1, 2$  and  $j = a, 1, \dots, m$ . The transformed process noise vector  $\tilde{\mathbf{w}}'$  is zero-mean, white with a power spectral density  $\tilde{\mathbf{Q}}'(t)$  such that

$$\begin{aligned} \tilde{\mathbf{Q}}' &= \text{diag} [\tilde{\mathbf{Q}}'_{s_a}, \tilde{\mathbf{Q}}'_{s_1}, \dots, \tilde{\mathbf{Q}}'_{s_m}, \tilde{\mathbf{Q}}'_{\text{clk},r}, \tilde{\mathbf{Q}}'_{\text{clk},s_1}, \dots, \tilde{\mathbf{Q}}'_{\text{clk},s_m}] \\ \tilde{\mathbf{Q}}'_{s_j} &= \Psi(\boldsymbol{\xi}_{s_j}) \text{diag} [0, 0, \tilde{q}_x, \tilde{q}_y] \Psi^\top(\boldsymbol{\xi}_{s_j}) \\ \Psi(\boldsymbol{\xi}_{s_j}) &\triangleq \begin{bmatrix} 0 & 0 & 0 & 0 \\ 0 & 0 & 0 & 0 \\ 0 & 0 & \cos \theta_{s_j} & \sin \theta_{s_j} \\ 0 & 0 & \frac{-\sin \theta_{s_j}}{r_{s_j}} & \frac{\cos \theta_{s_j}}{r_{s_j}} \end{bmatrix}, \quad j = a, 1, \dots, m \end{aligned}$$

$$\mathbf{H}' = \begin{bmatrix} \mathbf{h}'_{s_a}^\top & \mathbf{0} & \dots & \mathbf{0} & \mathbf{h}'_{\text{clk},r}^\top & \mathbf{0} & \dots & \mathbf{0} \\ \mathbf{0} & \mathbf{h}'_{s_1}^\top & \dots & \mathbf{0} & \mathbf{h}'_{\text{clk},r}^\top & \mathbf{h}'_{\text{clk},s_1}^\top & \dots & \mathbf{0} \\ \vdots & \vdots & \ddots & \vdots & \vdots & \vdots & \ddots & \vdots \\ \mathbf{0} & \mathbf{0} & \dots & \mathbf{h}'_{s_m}^\top & \mathbf{h}'_{\text{clk},r}^\top & \mathbf{0} & \dots & \mathbf{h}'_{\text{clk},s_m}^\top \end{bmatrix}$$

$$\mathbf{h}'_{s_j}^\top \triangleq [1, 0, 0, 0], \quad \mathbf{h}'_{\text{clk},r}^\top \triangleq [c, 0], \quad \mathbf{h}'_{\text{clk},s_j}^\top = -\mathbf{h}'_{\text{clk},r}^\top.$$

Next, the nonlinear dynamics in (8) is linearized around nominal  $\mathbf{x}^o_j$  and  $\mathbf{u}^o$  to yield the linear time-varying system

$$\frac{d}{dt} \delta \mathbf{x}'(t) = \mathbf{F}'(t) \delta \mathbf{x}'(t) + \mathbf{G}'(t) \delta \mathbf{u}(t) + \tilde{\mathbf{w}}'(t), \quad (9)$$

where  $\delta \mathbf{x}' \triangleq \mathbf{x}' - \mathbf{x}^o$  and  $\delta \mathbf{u} \triangleq \mathbf{u} - \mathbf{u}^o$ . It can be readily shown that  $\mathbf{F}'(t)$  is affine in the control inputs, namely

$$\mathbf{F}'(t) = \mathbf{F}'_0(t) + \sum_{i=1}^2 \mathbf{F}'_i(t) u_i(t)$$

$$\mathbf{F}'_0(t) = \text{diag} [\mathbf{F}'_{0,s_a}(t), \mathbf{F}'_{0,s_1}(t), \dots, \mathbf{F}'_{0,s_m}(t), \mathbf{A}_{\text{clks}}],$$

$$\mathbf{F}'_i(t) = \text{diag} [\mathbf{F}'_{i,s_a}(t), \mathbf{F}'_{i,s_1}(t), \dots, \mathbf{F}'_{i,s_m}(t), \mathbf{0}_{(2m+2) \times (2m+2)}]$$

$$\begin{aligned} \mathbf{F}'_{0,s_j}(t) &= \begin{bmatrix} 0 & 0 & 1 & 0 \\ 0 & 0 & 0 & 1 \\ \dot{\theta}_{s_j}^2 & 0 & 0 & 2r_{s_j} \dot{\theta}_{s_j} \\ \frac{2\dot{r}_{s_j} \dot{\theta}_{s_j}}{r_{s_j}^2} & 0 & \frac{-2\dot{\theta}_{s_j}}{r_{s_j}} & \frac{-2\dot{r}_{s_j}}{r_{s_j}} \end{bmatrix} \\ \mathbf{F}'_{1,s_j}(t) &= \begin{bmatrix} 0 & 0 & 0 & 0 \\ 0 & 0 & 0 & 0 \\ 0 & -\sin \theta_{s_j} & 0 & 0 \\ \frac{\sin \theta_{s_j}}{r_{s_j}^2} & \frac{-\cos \theta_{s_j}}{r_{s_j}} & 0 & 0 \end{bmatrix} \end{aligned}$$

$$\mathbf{F}'_{2,s_j}(t) = \begin{bmatrix} 0 & 0 & 0 & 0 \\ 0 & 0 & 0 & 0 \\ 0 & \cos \theta_{s_j} & 0 & 0 \\ \frac{-\cos \theta_{s_j}}{r_{s_j}^2} & \frac{-\sin \theta_{s_j}}{r_{s_j}} & 0 & 0 \end{bmatrix},$$

where  $j = a, 1, \dots, m$  and  $\mathbf{A}_{\text{clks}}$  is block-diagonal consisting of  $m+1$  blocks of  $\mathbf{A}_{\text{clk}}$ .

Then, the linearized system in (9) is discretized by assuming  $\mathbf{F}'(t)$ ,  $\mathbf{G}'(t)$ , and  $\tilde{\mathbf{Q}}'(t)$  to be approximately constant over a sampling interval  $T$ , i.e.,  $\mathbf{F}'(t) \approx \mathbf{F}'(k)$ ,  $\mathbf{G}'(t) \approx \mathbf{G}'(k)$ , and  $\tilde{\mathbf{Q}}'(t) \approx \tilde{\mathbf{Q}}'(k)$ , and assuming zero-order hold (ZOH) of the control inputs, i.e.,  $\{u(t) = u(k), k \leq t < k+1\}$  to yield [39]

$$\mathbf{x}'(k+1) = \Phi'(k+1, k) \mathbf{x}'(k) + \Gamma' \mathbf{u}(k) + \mathbf{w}'(k)$$

$$\Gamma'(k+1, k) \triangleq \int^{k+1} e^{\mathbf{F}'(k)[k+1-\tau]} \mathbf{G}'(k) d\tau,$$

$\Phi'(k+1, k) \triangleq e^{\mathbf{F}'(k)T}$ , and  $\mathbf{w}'(k)$  is a zero-mean white stochastic sequence with covariance  $\mathbf{Q}'(k+1, k)$  given by

$$\mathbf{Q}'(k+1, k) = \int^{k+1} e^{\mathbf{F}'(k)[k+1-\tau]} \tilde{\mathbf{Q}}'(k) e^{\mathbf{F}'^\top(k)[k+1-\tau]} d\tau.$$

Note that the state transition matrix  $\Phi'(k+1, k)$  is now a matrix exponential, since  $\mathbf{F}(t)$  is assumed to be constant over  $T$ . The matrix exponential can be factored as

$$\Phi'(k+1, k) = \Xi(k) e^{T \sum_{i=1}^2 \mathbf{F}'_i(k) u_i(k)}, \quad \Xi(k) \triangleq e^{T \mathbf{F}'_0(k)}.$$

Note that the above factorization holds, since the matrices  $\mathbf{F}'_0(k)$  and  $\sum_{i=1}^2 \mathbf{F}'_i(k) u_i(k)$  can be readily shown to be commutative (see Appendix A). Next, the matrix exponential  $e^{T \sum_{i=1}^2 \mathbf{F}'_i(k) u_i(k)}$  is expressed as a Taylor series and assuming sufficiently small values of  $T$ , the series is truncated to the first-order power in  $T$ . Therefore, the state transition matrix is expressible as

$$\Phi'(k+1, k) = \Xi(k) + T \sum_{i=1}^2 \Xi(k) \mathbf{F}'_i(k) u_i(k).$$

Proceeding in a similar manner for  $\mathbf{Q}'(k+1, k)$ , it is straightforward to show that  $\mathbf{Q}'(k+1, k) \approx T \mathbf{Q}'(k)$ .

Next, the predicted error covariance is given by

$$\begin{aligned} \mathbf{P}'(k+1|k) &= \Phi'(k+1, k) \mathbf{P}'(k|k) \Phi'^\top(k+1, k) \\ &\quad + \mathbf{Q}'(k+1, k). \end{aligned}$$

Note that to evaluate  $\mathbf{P}'(k+1|k)$ , which corresponds to the transformed state  $\mathbf{x}'(k)$ , one needs  $\mathbf{P}'(k|k)$  in the transformed state-space. Given the state estimate  $\hat{\mathbf{x}}(k|k)$  in the original state-space and associated  $\mathbf{P}(k|k)$ , one can find the transformed  $\mathbf{P}'(k|k)$  via linearization around  $\hat{\mathbf{x}}(k|k)$  as

$$\mathbf{x}' = \mathbf{g}(\mathbf{x}) \approx \mathbf{g}[\hat{\mathbf{x}}(k|k)] + \nabla_{\mathbf{x}} \mathbf{g}(\mathbf{x}) \Big|_{\mathbf{x}=\hat{\mathbf{x}}(k|k)} \cdot [\mathbf{x} - \hat{\mathbf{x}}(k|k)].$$

Recognizing that  $\text{cov}[\mathbf{x} - \hat{\mathbf{x}}(k|k)] = \mathbf{P}(k|k)$  and defining  $\Lambda(k) \triangleq \nabla_{\mathbf{x}} \mathbf{g}(\mathbf{x})|_{\mathbf{x}=\hat{\mathbf{x}}(k|k)}$ , yields

$$\mathbf{P}'(k+1|k) = \Lambda(k) \mathbf{P}(k+1|k) \Lambda^\top(k). \quad (10)$$

Explicit expression for  $\Lambda(k)$  is given in Appendix B.

Substituting for  $\Phi'(k+1, k)$  and truncating to the first-order power in  $T$ , it can be shown that the predicted error covariance is affine in the control inputs, specifically

$$\mathbf{P}'(k+1|k) = \mathbf{P}'_0(k+1|k) + \sum_{i=1}^2 \mathbf{P}'_i(k+1|k)u_i(k)$$

$$\mathbf{P}'_0(k+1|k) \triangleq \Xi(k)\mathbf{P}'(k|k)\Xi^T(k) + \mathbf{Q}'(k+1, k)$$

$$\mathbf{P}'_i(k+1|k) \triangleq T \left[ \Xi(k)\mathbf{P}'(k|k)\mathbf{F}'_i^T(k)\Xi^T(k) + \Xi(k)\mathbf{F}'_i(k)\mathbf{P}'(k|k)\Xi^T(k) \right], \quad i = 1, 2.$$

Finally, the observation innovation  $\tilde{z}'(k+1) \triangleq z(k+1) - \hat{z}'(k+1|k)$ , where  $\hat{z}'(k+1|k) = \mathbf{H}'\hat{\mathbf{x}}'(k+1|k)$ , has a corresponding covariance  $\mathbf{S}'(k+1)$  given by

$$\mathbf{S}'(k+1) = \mathbf{H}'\mathbf{P}'(k+1|k)\mathbf{H}'^T + \mathbf{R},$$

and (7) follows with  $\mathbf{S}'_0(k+1) = \mathbf{H}\mathbf{P}'_0(k+1|k)\mathbf{H}^T + \mathbf{R}$  and  $\mathbf{S}'_i(k+1) = \mathbf{H}\mathbf{P}'_i(k+1|k)\mathbf{H}^T$ , for  $i = 1, 2$ . ■

The special affine form of the innovation matrix in (7) yields the following result regarding the optimal solution of the innovation-based optimization problems.

**Theorem III.2.** *The optimal solutions for the innovation-based greedy motion planning problems: MILD, MIT, and MIME lie on the extreme points of the feasibility region.*

*Proof:* First, it is easy to see that the velocity and acceleration constraints are convex in the optimization variable  $\mathbf{u}(k)$ , since the norm of a vector is convex and the composition of a convex function with an affine mapping preserves convexity [40]. Next, we show that MILD is a concave function, whereas MIT and MIME are convex functions. To this end, concavity of MILD follows from Lemma C.1 in Appendix C. Moreover, since MIT is affine in the optimization variable, it is both convex and concave. Convexity of MIME follows from Lemma C.2 in Appendix C. Hence, in the MILD case, one is maximizing a concave functional subject to convex constraints. But, since the logarithm functional is strictly monotonically increasing, the maximum is attained at the extreme points of the feasibility region. In the MIT and MIME case, one is maximizing convex functionals subject to convex constraints; therefore, the maximum is attained at the extreme points of the feasibility region [41]. ■

The significance of Theorem III.2 is that the innovation-based optimization problems reduce to search problems via function evaluations. Figure 3(a) illustrates the control feasibility region over which the information- and innovation-based optimization functionals need to be considered. Figure 3(b) illustrates the extreme points of the feasibility region over which the optimal solution of the innovation-based functionals lies, which can be found straightforwardly.

#### E. Relationship between D-Optimality and MILD

Under linear Gaussian assumptions, one can show that D-optimality and MILD are equivalent. To see this, consider two jointly Gaussian random vectors  $\mathbf{x}$  and  $\mathbf{z}$  with auto- and cross-covariances given by  $\mathbf{P}_{\mathbf{x}\mathbf{x}}$ ,  $\mathbf{P}_{\mathbf{z}\mathbf{z}}$ , and  $\mathbf{P}_{\mathbf{x}\mathbf{z}}$ . Assume that  $\mathbf{z} =$

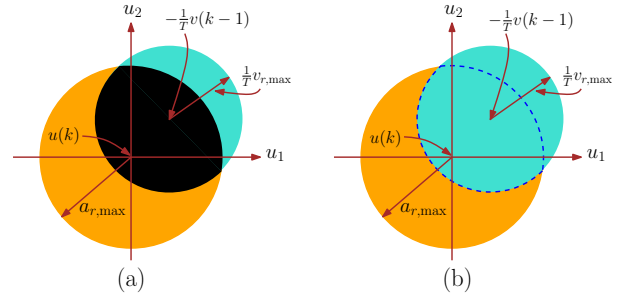


Fig. 3. (a) Black shaded region: control feasibility region for information- and innovation-based optimization. (b) Dashed curve: extreme points of feasibility region over which optimal solution of innovation-based optimization lies.

$\mathbf{H}\mathbf{x} + \mathbf{v}$ , where  $\mathbf{v} \sim \mathcal{N}(\mathbf{0}, \mathbf{R})$  is independent of  $\mathbf{x}$ . Then, the mutual information between  $\mathbf{x}$  and  $\mathbf{z}$ , which measures the expected reduction in entropy in one random vector due to the observation of another, can be shown through the Kullback-Leibler divergence to be given by [42]

$$I(\mathbf{x}, \mathbf{z}) = \frac{1}{2} \log \frac{\det[\mathbf{P}_{\mathbf{x}\mathbf{x}}^{-1} + \mathbf{H}^T \mathbf{R}^{-1} \mathbf{H}]}{\det[\mathbf{P}_{\mathbf{x}\mathbf{x}}^{-1}]} \quad (11)$$

$$= \frac{1}{2} \log \frac{\det[\mathbf{H}\mathbf{P}_{\mathbf{x}\mathbf{x}}\mathbf{H}^T + \mathbf{R}]}{\det[\mathbf{R}]} \quad (12)$$

Therefore, to maximize  $I(\mathbf{x}, \mathbf{z})$  one can either maximize the right-hand side of (11) or (12). Interpreting  $\mathbf{P}_{\mathbf{x}\mathbf{x}}$  as the prediction error covariance, which is not a function of  $\mathbf{u}$  as shown in Subsection III-C, it can be established that the former maximization is nothing but D-optimality, while the latter maximization is MILD.

## IV. SIMULATION RESULTS

This section presents simulation results comparing the greedy information- and innovation-based receiver motion strategies. A receiver with an unknown initial state vector was assumed to be dropped in an OpNav environment comprising an anchor SOP with a known initial state vector, labeled  $\text{SOP}_a$ , and three SOPs with unknown initial state vectors, labeled  $\{\text{SOP}_i\}_{i=1}^3$ . The receiver's and SOPs' clocks were assumed to be temperature-compensated and oven-controlled crystal oscillators (TCXO and OCXOs), respectively. For purposes of numerical stability, the clock error states were defined to be  $c\delta t$  and  $c\dot{\delta}t$ . The simulation settings are given in Table I.

Eight receiver trajectories were simulated. The first two were open-loop: one in which the receiver's maneuvers were chosen randomly at each time step from the feasibility region, while in the other, the maneuvers were specified so to traverse a trajectory around  $\text{SOP}_a$ . The remaining six trajectories were closed-loop according to Figure 1 with  $\mathcal{J}[\mathbf{u}(k)]$  being D-optimality, A-optimality, E-optimality, MILD, MIT, and MIME. To avoid converging to a local minimum, the optimal solutions of the information-based functionals were found by gridding the control feasibility region and performing an exhaustive-search, instead of solving through general-purpose numerical optimization solvers. On the other hand, the optimal solutions of the innovation-based functionals were found by searching over the extreme points of the feasibility region. For

the same gridding resolution, the innovation-based methods were thirty times faster than the information-based. Figure 4 illustrates the trajectories for a single simulation run.

TABLE I  
SIMULATION SETTINGS

Parameter	Value
$\mathbf{x}_r(0)$	$[0, 0, 0, 0, 100, 10]^T$
$\mathbf{x}_{s_a}(0)$	$[0, 150, 10, 0.1]^T$
$\mathbf{x}_{s_1}(0)$	$[100, -150, 20, 0.2]^T$
$\mathbf{x}_{s_2}(0)$	$[200, 200, 30, 0.3]^T$
$\mathbf{x}_{s_3}(0)$	$[-150, 50, 40, 0.4]^T$
$\hat{\mathbf{x}}_r(0 -1)$	$\sim \mathcal{N}[\mathbf{x}_r(0), \mathbf{P}_r(0 -1)]$
$\hat{\mathbf{x}}_{s_i}(0 -1)$	$\sim \mathcal{N}[\mathbf{x}_{s_i}(0), \mathbf{P}_{s_i}(0 -1)], i = 1, 2, 3$
$\mathbf{P}_r(0 -1)$	$(10^4) \cdot \text{diag}[1, 1, 10^{-2}, 10^{-2}, 1, 10^{-2}]$
$\mathbf{P}_{s_i}(0 -1)$	$(10^3) \cdot \text{diag}[1, 1, 1, 10^{-1}], i = 1, 2, 3$
$\{h_{0,r}, h_{-2,r}\}$	$\{2 \times 10^{-19}, 2 \times 10^{-20}\}$
$\{h_{0,s_j}, h_{-2,s_j}\}$	$\{8 \times 10^{-20}, 4 \times 10^{-23}\}, j = a, 1, 2, 3$
$\tilde{q}_x, \tilde{q}_y$	$0.1 \text{ (m/s}^2\text{)}^2$
$\mathbf{R}$	$\text{diag}[400, 500, 600, 700] \text{ m}^2$
$\{v_{\max}, a_{\max}\}$	$\{20 \text{ m/s}, 5 \text{ m/s}^2\}$
$T$	$0.1 \text{ s}$

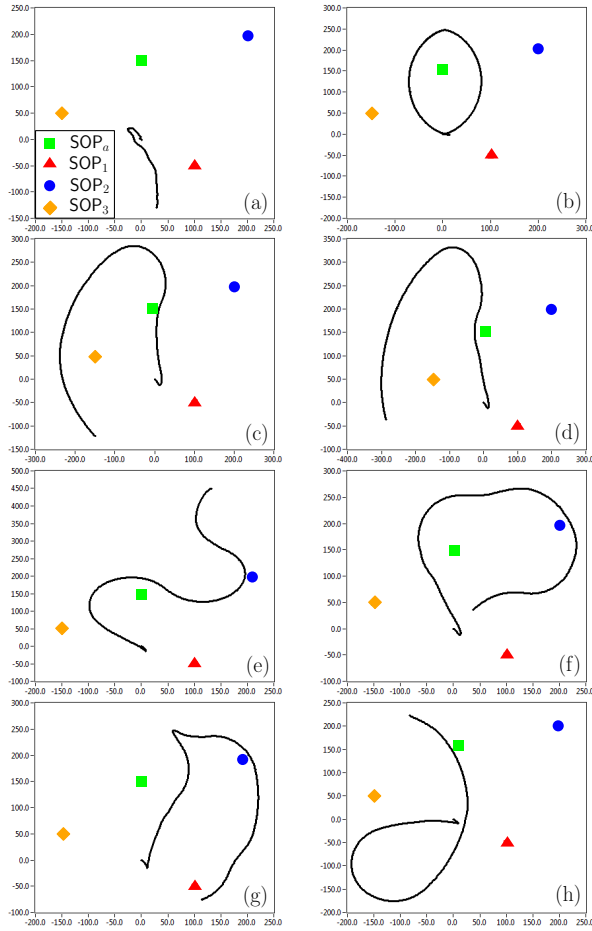


Fig. 4. Receiver trajectories due to (a) random, (b) prescribed, (c) D-optimality, (d) MILD, (e) A-optimality, (f) MIT, (g) E-optimality, and (h) MIME motion planning strategies.

To compare the performance of the eight trajectories, the root mean squared estimation error (RMSEE) criterion was chosen. Figures 5-11 show the RMSEE for 100 MC runs for

the receiver and  $\text{SOP}_1$  along with the total RMSEE over the simulation horizon (50 seconds). Similar RMSEE and total RMSEE results were reported for  $\text{SOP}_2$  and  $\text{SOP}_3$ .

The following conclusions can be drawn from these results. First, optimization-based motion planning yielded superior results to open-loop random and predefined trajectories, which highlights the need to optimize the receiver trajectory for optimal information gathering. Second, there was a consistent performance ordering of the optimization-based methods: D-optimality and MILD yielded the best results, followed by A-optimality and MIT, while E-optimality and MIME yielded the worst results. Note that the only exception to this ordering was in the receiver and SOP clock drift RMSEE for A-optimality, E-optimality, MIT, and MIME. Nevertheless, the differences among these four methods for the clock drift states RMSEE were practically negligible. Third, while D-optimality and MILD were comparable, D-optimality was slightly superior, despite the fact that they were shown to be equivalent under certain assumptions in Subsection III-E. This can be explained by recalling that in deriving MILD, some simplifying assumptions were invoked, namely dropping terms involving higher-order powers of  $T$  and approximating the matrix exponential via a Taylor Series expansion. Additionally, D-optimality and MILD equivalency was shown to hold for the Gaussian case, which does not hold here due to the nonlinearity in the observations.

## V. CONCLUSIONS

This paper studied the following problem. A receiver with no *a priori* knowledge about its own states is dropped in an OpNav environment comprising multiple terrestrial SOPs. The receiver has no *a priori* knowledge of the state vectors of these SOPs, except for one anchor SOP. The receiver draws pseudorange observations from the SOPs. Assuming that the receiver can prescribe its maneuvers, what greedy motion planning strategy should the receiver adopt to build a high-fidelity signal landscape map of the environment while simultaneously localizing itself within this map in time and space with high accuracy? Six information- and innovation-based optimization measures were derived. On one hand, it was demonstrated that the information-based measures did not possess convexity properties, which necessitates relying on general-purpose numerical constrained nonlinear optimization solvers. On the other hand, under suitable reformulations and mild approximations, it was shown that the innovation-based measures possessed strong convexity properties, which reduced solving the associated optimization problems to searching over the extreme points of the feasibility regions. Numerical simulation results were presented comparing the six strategies and two open-loop strategies in terms of the RMSEE. It was demonstrated that all six strategies outperformed the two open-loop strategies. Among the six strategies, D-optimality and MILD performed the best, followed by A-optimality and MIT, followed by E-optimality and MIME. Future work will study the analytical connections between A-optimality and between MIT and E-optimality and MIME. Also, distributivity properties of MILD, MIT, and MIME will be explored for the case of multiple receivers.

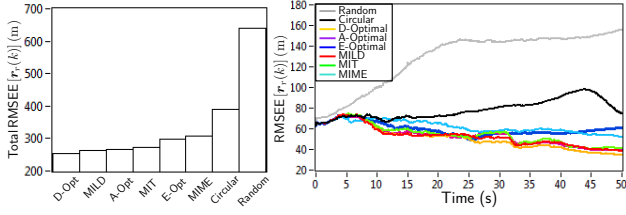


Fig. 5. Receiver position RMSEE and total RMSEE

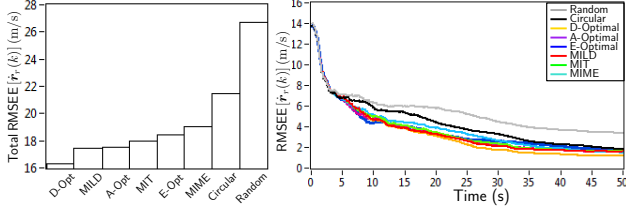


Fig. 6. Receiver velocity RMSEE and total RMSEE

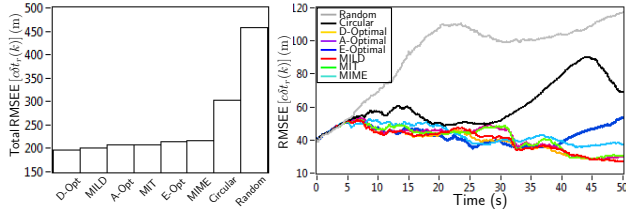


Fig. 7. Receiver clock bias RMSEE and total RMSEE

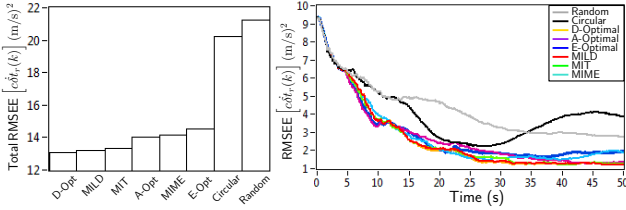
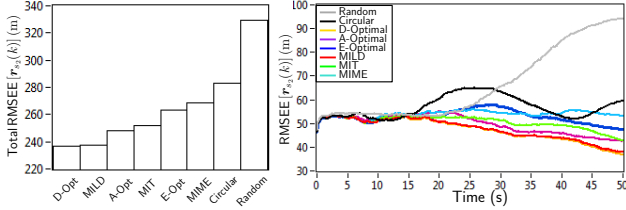
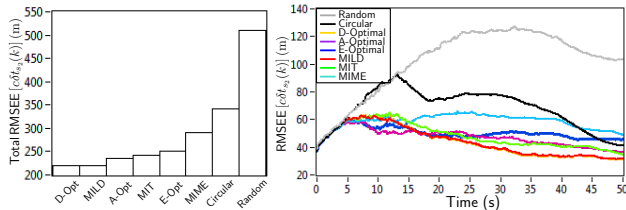
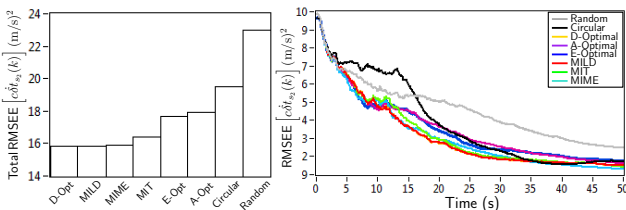


Fig. 8. Receiver clock drift RMSEE and total RMSEE


 Fig. 9. SOP<sub>1</sub> position RMSEE and total RMSEE

 Fig. 10. SOP<sub>1</sub> clock bias RMSEE and total RMSEE

 Fig. 11. SOP<sub>1</sub> clock drift RMSEE and total RMSEE

## APPENDIX A

## COMMUTATIVITY OF DYNAMICS MATRICES

**Fact A.1.** The matrices  $\mathbf{F}'_0$  and  $\sum_{i=1}^2 \mathbf{F}_i u_i$  are commutative.

*Proof:* Denoting  $\mathbf{A} \triangleq \mathbf{F}'_0$  and  $\mathbf{B} \triangleq \sum_{i=1}^2 \mathbf{F}_i u_i$ , direct calculations reveal that

$$\mathbf{AB} = \mathbf{BA} = \text{diag} [\mathbf{F}'_{3,s_a}, \mathbf{F}'_{3,s_1}, \dots, \mathbf{F}'_{3,s_m}, \mathbf{0}_{(2m+2) \times (2m+2)}],$$

$$\mathbf{F}'_{3,s_j} = \begin{bmatrix} 0 & 0 & 0 & 0 \\ 0 & 0 & 0 & 0 \\ 0 & 0 & 0 & 0 \\ \frac{2\dot{r}_{s_j}\dot{\theta}_{s_j}(u_1 \sin \theta_{s_j} - u_2 \cos \theta_{s_j})}{r_{s_j}^3} & 0 & 0 & 0 \end{bmatrix},$$

where  $j = a, 1, \dots, m$ . ■

## APPENDIX B

## MATRIX BLOCKS FOR EQUATION (10)

$$\mathbf{\Lambda}(k) = \begin{bmatrix} \mathbf{\Lambda}_{s_a} & \mathbf{0}_{4 \times 4} & \cdots & \mathbf{0}_{4 \times 4} \\ \mathbf{\Lambda}_{s_1} & -\mathbf{\Lambda}_{s_1} & \cdots & \mathbf{0}_{4 \times 4} \\ \vdots & \vdots & \ddots & \vdots \\ \mathbf{\Lambda}_{s_m} & \mathbf{0}_{4 \times 4} & \cdots & -\mathbf{\Lambda}_{s_m} \\ \mathbf{\Lambda}_{\text{clk},r} & \mathbf{0}_{2 \times 4} & \cdots & \mathbf{0}_{2 \times 4} \\ \mathbf{0}_{2 \times 4} & \mathbf{\Lambda}_{\text{clk},s_1} & \cdots & \mathbf{0}_{2 \times 4} \\ \vdots & \vdots & \ddots & \vdots \\ \mathbf{0}_{2 \times 4} & \mathbf{0}_{2 \times 4} & \cdots & \mathbf{\Lambda}_{\text{clk},s_m} \end{bmatrix}.$$

$$\mathbf{\Lambda}_{s_j} \triangleq \begin{bmatrix} \mathbf{\Lambda}_{r_{s_j},x_r} & \mathbf{\Lambda}_{r_{s_j},y_r} & 0 & 0 & 0 & 0 \\ \mathbf{\Lambda}_{\theta_{s_j},x_r} & \mathbf{\Lambda}_{\theta_{s_j},y_r} & 0 & 0 & 0 & 0 \\ \mathbf{\Lambda}_{\dot{r}_{s_j},x_r} & \mathbf{\Lambda}_{\dot{r}_{s_j},y_r} & \mathbf{\Lambda}_{\dot{r}_{s_j},\dot{x}_r} & \mathbf{\Lambda}_{\dot{r}_{s_j},\dot{y}_r} & 0 & 0 \\ \mathbf{\Lambda}_{\dot{\theta}_{s_j},x_r} & \mathbf{\Lambda}_{\dot{\theta}_{s_j},y_r} & \mathbf{\Lambda}_{\dot{\theta}_{s_j},\dot{x}_r} & \mathbf{\Lambda}_{\dot{\theta}_{s_j},\dot{y}_r} & 0 & 0 \end{bmatrix}$$

$$\mathbf{\Lambda}_{r_{s_j},x_r} = \mathbf{\Lambda}_{\dot{r}_{s_j},\dot{x}_r} = \frac{x_r - x_{s_j}}{\|\mathbf{r}_r - \mathbf{r}_{s_j}\|}, \quad \mathbf{\Lambda}_{r_{s_j},y_r} = \mathbf{\Lambda}_{\dot{r}_{s_j},\dot{y}_r} = \frac{y_r - y_{s_j}}{\|\mathbf{r}_r - \mathbf{r}_{s_j}\|}$$

$$\mathbf{\Lambda}_{\theta_{s_j},x_r} = \mathbf{\Lambda}_{\dot{\theta}_{s_j},\dot{x}_r} = \frac{-y_r + y_{s_j}}{\|\mathbf{r}_r - \mathbf{r}_{s_j}\|^2}, \quad \mathbf{\Lambda}_{\theta_{s_j},y_r} = \mathbf{\Lambda}_{\dot{\theta}_{s_j},\dot{y}_r} = \frac{x_r - x_{s_j}}{\|\mathbf{r}_r - \mathbf{r}_{s_j}\|^2}$$

$$\mathbf{\Lambda}_{\dot{r}_{s_j},x_r} = \frac{[\dot{y}_r(-x_r + x_{s_j}) + \dot{x}_r(y_r - y_{s_j})](y_r - y_{s_j})}{\|\mathbf{r}_r - \mathbf{r}_{s_j}\|^3}$$

$$\mathbf{\Lambda}_{\dot{r}_{s_j},y_r} = \frac{[\dot{y}_r(x_r - x_{s_j}) + \dot{x}_r(-y_r + y_{s_j})](x_r - x_{s_j})}{\|\mathbf{r}_r - \mathbf{r}_{s_j}\|^3}$$

$$\mathbf{\Lambda}_{\dot{\theta}_{s_j},x_r} = \left\{ \dot{y}_r [-(x_r - x_{s_j})^2 + (y_r - y_{s_j})^2] + 2\dot{x}_r(x_r - x_{s_j})(y_r - y_{s_j}) \right\} / \|\mathbf{r}_r - \mathbf{r}_{s_j}\|^2$$

$$\mathbf{\Lambda}_{\dot{\theta}_{s_j},y_r} = \left\{ \dot{x}_r [-(x_r - x_{s_j})^2 + (y_r - y_{s_j})^2] - 2\dot{y}_r(x_r - x_{s_j})(y_r - y_{s_j}) \right\} / \|\mathbf{r}_r - \mathbf{r}_{s_j}\|^2$$

$$\mathbf{\Lambda}_{\text{clk},r} \triangleq \begin{bmatrix} \mathbf{0}_{2 \times 4} & \mathbf{I}_{2 \times 2} \end{bmatrix}$$

$$\mathbf{\Lambda}_{\text{clk},s_j} \triangleq \begin{bmatrix} \mathbf{0}_{2 \times 2} & \mathbf{I}_{2 \times 2} \end{bmatrix}, \quad j = a, 1, \dots, m.$$

## APPENDIX C

## LINEAR FUNCTIONALS CONVEXITY PROPERTIES

**Lemma C.1.** *The functional  $f(\mathbf{x}) = \log [\det (\mathbf{A}_0 + \sum_{i=1}^n x_i \mathbf{A}_i)]$ , where  $\mathbf{x} \in \mathbb{R}^n$  and  $\mathbf{A}_i \in \mathbb{S}^m$  is concave on  $\{\mathbf{x} : \mathbf{A}_0 + \sum_{i=1}^n x_i \mathbf{A}_i \succ 0\}$ .*

*Proof:* Since nonnegative weighting of a concave functional preserves its concavity, consider the functional

$$\begin{aligned} f(\mathbf{x}) &= \frac{1}{m} \log \left[ \det \left( \mathbf{A}_0 + \sum_{i=1}^n x_i \mathbf{A}_i \right) \right] \\ &= \log \left\{ \left[ \det \left( \mathbf{A}_0 + \sum_{i=1}^n x_i \mathbf{A}_i \right) \right]^{\frac{1}{m}} \right\} \\ &\triangleq h[g(\mathbf{x})] \end{aligned}$$

Using the fact that the functional  $g'(\mathbf{x}) = -[\det (\mathbf{A}_0 + \sum_{i=1}^n x_i \mathbf{A}_i)]^{\frac{1}{m}}$ , where  $\mathbf{x} \in \mathbb{R}^n$  and  $\mathbf{A}_i \in \mathbb{S}^m$  is convex on  $\{\mathbf{x} : \mathbf{A}_0 + \sum_{i=1}^n x_i \mathbf{A}_i \succ 0\}$ ; hence,  $g(\mathbf{x}) \triangleq -g'(\mathbf{x})$  is concave. Recognizing that  $h$  is concave and nondecreasing, we conclude that  $f$  is concave, from applying the composition rule: if  $f(\mathbf{x}) \triangleq h[g(\mathbf{x})]$ , with  $h : \mathbb{R} \rightarrow \mathbb{R}$  and  $g : \mathbb{R}^n \rightarrow \mathbb{R}$ , then  $f$  is concave if  $h$  is concave and nondecreasing and  $g$  is concave [40]. ■

**Lemma C.2.** *The functional  $f(\mathbf{x}) = \lambda_{\max} [\mathbf{A}_0 + \sum_{i=1}^n x_i \mathbf{A}_i]$ , where  $\mathbf{x} \in \mathbb{R}^n$  and  $\mathbf{A}_i \in \mathbb{S}^n$  is convex.*

*Proof:* The functional  $f$  can be expressed as

$$f(\mathbf{x}) = \sup_{\|\mathbf{y}\|_2=1} \left[ \mathbf{y}^T \left( \mathbf{A}_0 + \sum_{i=1}^n x_i \mathbf{A}_i \right) \mathbf{y} \right].$$

Since  $f$  is the point-wise supremum of a family of linear functionals of  $\mathbf{x}$ , i.e.  $\mathbf{y}^T (\mathbf{A}_0 + \sum_{i=1}^n x_i \mathbf{A}_i) \mathbf{y}$ , indexed by  $\mathbf{y} \in \mathbb{R}^n$ , and using the fact that the point-wise supremum of convex functionals is convex, then  $f$  is convex. ■

## ACKNOWLEDGMENT

The authors would like to thank Jahshan Bhatti and Professor Behcet Acikmese for their helpful discussions.

## REFERENCES

- [1] M. Endsley, "Toward a theory of situation awareness in dynamic systems," *Human Factors: The Journal of the Human Factors and Ergonomics Society*, vol. 37, no. 1, pp. 32–64, March 1995.
- [2] G. Seco-Granados, J. Lopez-Salcedo, D. Jimenez-Banos, and G. Lopez-Risueno, "Challenges in indoor global navigation satellite systems: Unveiling its core features in signal processing," *IEEE Signal Processing Magazine*, vol. 29, no. 2, pp. 108–131, March 2012.
- [3] T. Humphreys, "Detection strategy for cryptographic GNSS anti-spoofing," *IEEE Transactions on Aerospace and Electronic Systems*, vol. 49, no. 2, pp. 1073–1090, April 2013.
- [4] A. Soloviev and F. Van Graas, "Use of deeply integrated GPS/INS architecture and laser scanners for the identification of multipath reflections in urban environments," *IEEE Journal of Selected Topics in Signal Processing*, vol. 3, no. 5, pp. 786–797, October 2009.
- [5] R. Toledo-Moreo, D. Betaille, F. Peyret, and J. Leneurit, "Fusing GNSS, dead-reckoning, and enhanced maps for road vehicle lane-level navigation," *IEEE Journal of Selected Topics in Signal Processing*, vol. 3, no. 5, pp. 798–809, October 2009.
- [6] R. Martin, J. Velotta, and J. Raquet, "Bandwidth efficient cooperative TDOA computation for multicarrier signals of opportunity," *IEEE Transactions on Signal Processing*, vol. 57, no. 6, pp. 2311–2322, June 2009.
- [7] K. Pesyna, Z. Kassas, J. Bhatti, and T. Humphreys, "Tightly-coupled opportunistic navigation for deep urban and indoor positioning," in *Proceedings of ION GNSS*, September 2011, pp. 3605–3617.
- [8] C. Yang, T. Nguyen, E. Blasch, and D. Qiu, "Assessing terrestrial wireless communications and broadcast signals as signals of opportunity for positioning and navigation," in *Proceedings of the ION GNSS*, Sep. 2012.
- [9] M. Rabinowitz and J. Spilker, J.J., "A new positioning system using television synchronization signals," *IEEE Transactions on Broadcasting*, vol. 51, no. 1, pp. 51–61, March 2005.
- [10] K. Pesyna, Z. Kassas, and T. Humphreys, "Constructing a continuous phase time history from TDMA signals for opportunistic navigation," in *Proceedings of IEEE/ION Position Location and Navigation Symposium (PLANS)*, April 2012, pp. 1209–1220.
- [11] R. Martin, C. Yan, H. Fan, and C. Rondeau, "Algorithms and bounds for distributed TDOA-based positioning using OFDM signals," *IEEE Transactions on Signal Processing*, vol. 59, no. 3, pp. 1255–1268, March 2011.
- [12] Z. Kassas, "Collaborative opportunistic navigation," *IEEE Aerospace and Electronic Systems Magazine*, vol. 28, no. 6, pp. 38–41, June 2013.
- [13] H. Durrant-Whyte and T. Bailey, "Simultaneous localization and mapping: part I," *IEEE Robotics & Automation Magazine*, vol. 13, no. 2, pp. 99–110, June 2006.
- [14] T. Bailey and H. Durrant-Whyte, "Simultaneous localization and mapping: part II," *IEEE Robotics & Automation Magazine*, vol. 13, no. 3, pp. 108–117, September 2006.
- [15] Z. Kassas and T. Humphreys, "Observability analysis of opportunistic navigation with pseudorange measurements," in *Proceedings of AIAA Guidance, Navigation, and Control Conference (GNC)*, August 2012, pp. 4760–4775.
- [16] —, "Observability analysis of collaborative opportunistic navigation with pseudorange measurements," *IEEE Transactions on Intelligent Transportation Systems*, vol. 15, no. 1, pp. 260–273, February 2014.
- [17] —, "Observability and estimability of collaborative opportunistic navigation with pseudorange measurements," in *Proceedings of ION GNSS*, September 2012, pp. 621–630.
- [18] —, "Receding horizon trajectory optimization in opportunistic navigation environments," *IEEE Transactions on Aerospace and Electronic Systems*, 2014, submitted.
- [19] Y. Oshman and P. Davidson, "Optimization of observer trajectories for bearings-only target localization," *IEEE Transactions on Aerospace and Electronic Systems*, vol. 35, no. 3, pp. 892–902, July 1999.
- [20] K. Zhou and S. Roumeliotis, "Optimal motion strategies for range-only constrained multisensor target tracking," *IEEE Transactions on Robotics*, vol. 24, no. 5, pp. 1168–1185, October 2008.
- [21] R. Pitre, X. Li, and R. R. Delbalzo, "UAV route planning for joint search and track missions—an information-value approach," *IEEE Transactions on Aerospace and Electronic Systems*, vol. 48, no. 3, pp. 2551–2565, July 2012.
- [22] H. Feder, J. Leonard, and C. Smith, "Adaptive mobile robot navigation and mapping," *International Journal of Robotics Research*, vol. 18, no. 7, pp. 650–668, July 1999.
- [23] C. Leung, S. Huang, N. Kwok, and G. Dissanayake, "Planning under uncertainty using model predictive control for information gathering," *Robotics and Autonomous Systems*, vol. 54, no. 11, pp. 898–910, November 2006.
- [24] M. Bryson and S. Sukkarieh, "Observability analysis and active control for airborne SLAM," *IEEE Transactions on Aerospace and Electronic Systems*, vol. 44, no. 1, pp. 261–280, Jan. 2008.
- [25] Z. Kassas and T. Humphreys, "Motion planning for optimal information gathering in opportunistic navigation systems," in *Proceedings of AIAA Guidance, Navigation, and Control Conference (GNC)*, August 2013, 551–4565.
- [26] Z. Kassas, J. Bhatti, and T. Humphreys, "Receding horizon trajectory optimization for simultaneous signal landscape mapping and receiver localization," in *Proceedings of ION GNSS*, Nashville, Tennessee, September 2013, pp. 1962–1969.
- [27] Z. Kassas and T. Humphreys, "The price of anarchy in active signal landscape map building," in *IEEE Global Signal and Information Processing*, Austin, Texas, December 2013, pp. 165–168.
- [28] A. Davison and D. Murray, "Simultaneous localization and map-building using active vision," *IEEE Transactions on Pattern Analysis and Machine Intelligence*, vol. 24, no. 7, pp. 865–880, 2002.
- [29] A. Davison, "Real-time simultaneous localisation and mapping with a single camera," in *IEEE International Conference on Computer Vision*, vol. 2, 2003, pp. 1403–1410.

- [30] A. Thompson, J. Moran, and G. Swenson, *Interferometry and Synthesis in Radio Astronomy*, 2nd ed. John Wiley, 2001.
- [31] Y. Bar-Shalom, X. Li, and T. Kirubarajan, *Estimation with Applications to Tracking and Navigation*. New York, NY: John Wiley, 2002.
- [32] Z. Kassas, "Numerical simulation of continuous-time stochastic dynamical systems with noisy measurements and their discrete-time equivalents," in *IEEE International Symposium on Computer-Aided Control System Design (CACSD)*, September 2011, pp. 1397–1402.
- [33] M. Psiaki and S. Mohiuddin, "Modeling, analysis, and simulation of GPS carrier phase for spacecraft relative navigation," *Journal of Guidance, Control, and Dynamics*, vol. 30, no. 6, pp. 1628–1639, November–December 2007.
- [34] W. Cochran, "Experiments for nonlinear functions," *Journal of the American Statistical Association*, vol. 68, no. 344, pp. 771–781, December 1973.
- [35] H. Durrant-Whyte, *Multi Sensor Data Fusion*, 2001.
- [36] T. Cover and J. Thomas, *Elements of Information Theory*, 2nd ed. Wiley-Interscience, 2006.
- [37] D. Uciński, *Optimal Measurement Methods for Distributed Parameter System Identification*. CRC Press, 2005.
- [38] M. Grant and S. Boyd, "CVX: Matlab software for disciplined convex programming, version 2.0 beta," <http://cvxr.com/cvx>, September 2013.
- [39] J. Mendel, *Lessons in Estimation Theory for Signal Processing, Communications, and Control*, 2nd ed. Prentice Hall, 1995.
- [40] S. Boyd and L. Vandenberghe, *Convex Optimization*. Cambridge University Press, 2004.
- [41] R. Baldick, *Applied Optimization*. Cambridge University Press, 2006.
- [42] J. Williams, "Information theoretic sensor management," Ph.D. dissertation, Massachusetts Institute of Technology, USA, 2007.

PLACE  
PHOTO  
HERE

and integrity.

**Todd E. Humphreys** (M'12) received a B.S. and M.S. in Electrical and Computer Engineering from Utah State University and a Ph.D. in Aerospace Engineering from Cornell University. He is currently an assistant professor in the department of Aerospace Engineering and Engineering Mechanics at the University of Texas at Austin and Director of the University of Texas Radionavigation Laboratory. His research interests are in estimation and filtering, GNSS technology, GNSS-based study of the ionosphere and neutral atmosphere, and GNSS security

PLACE  
PHOTO  
HERE

**Zaher (Zak) M. Kassas** (S'98-M'08-SM'011) received a B.E. with Honors in Electrical Engineering from The Lebanese American University, a M.S. in Electrical and Computer Engineering from The Ohio State University, and a M.S.E. in Aerospace Engineering from The University of Texas at Austin. He is currently a Ph.D. candidate at The University of Texas at Austin. From 2004 to 2010 he was a research and development engineer with the Control Design and Dynamical Systems Simulation Group at National Instruments Corp. From 2008 to 2011

he was an adjunct professor at Texas State University. His research interests include estimation, navigation, autonomous systems, and ITS.

PLACE  
PHOTO  
HERE

**Ari Arapostathis** (F'07) received the B.S. degree from Massachusetts Institute of Technology, Cambridge, and the Ph.D. degree from the University of California, Berkeley. He has been a Faculty Member with The University of Texas at Austin since 1982. His research interests include analysis and estimation techniques for stochastic systems, the application of differential geometric methods to the design and analysis of control systems, stability properties of large-scale interconnected power systems, and stochastic and adaptive control theory.